Available online at www.sciencedirect.com
ScienceDirect
Journal of Molecular Catalysis A: Chemical 286 (2008) 79–86
JOURNAL OF MOLECULAR CATALYSIS A: CHEMICAL
www.elsevier.com/locate/molcata

Oxygen permeation and oxidative coupling of methane in membrane reactor: A new facile synthesis method for selective perovskite catalyst

Z. Taheri [a,b], K. Nazari [a,*], A.A. Safekordi [c], N. Seyed-Matin [a], R. Ahmadi [a], N. Esmaeili [a], A. Tofigh [a]

[a] *Research Institute of Petroleum Industry, P.O. Box 18745/4163, Tehran, Iran*
[b] *Science & Research Campus, Islamic Azad University, Tehran, Iran*
[c] *Faculty of Chemical Engineering, Sharif University of Technology, Tehran, Iran*

Received 25 November 2007; received in revised form 16 January 2008; accepted 31 January 2008
Available online 9 February 2008

Abstract

A dense membrane of $La_{0.6}Sr_{0.4}Co_{0.8}Fe_{0.2}O_{3-\delta}$ (LSCF) perovskite was prepared by a new chelating agent, ethylene diamine *N*,*N*,*N*′,*N*′-tetra *N*-acetyl diamine (EDTNAD). As a potent ligand, EDTNAD provided a facile one-step method to form complexes of the four metal ions, simultaneously. The oxygen permeation flux through the pure perovskite LSCF dense membrane was measured over temperature range of 1073–1223 K, thickness of 0.7–1.0 mm and oxygen partial pressure of 0.1–1.0 bar. Oxidative coupling of methane (OCM) reaction using LSCF disk in the atmospheric membrane reactor and over the temperature range of 1073–1173 K showed a C_2 selectivity of 100% and C_2 yield of 5.01% at 1153 K. Furthermore, OCM reaction data of the membrane reactor were discussed and compared with those of the fixed bed using the same perovskite powder as the catalyst.

Keywords: Perovskite; Membrane reactor; Oxygen permeation; OCM; Selectivity

1. Introduction

Nowadays, due to the existence of huge gas resources, methane conversion to valuable products is of paramount importance. Oxidative coupling of methane (OCM) to C_2 hydrocarbons (ethane and ethylene) is a well-known conversion process. Although enhancing the C_2 selectivity and yield was followed by others until 1990 [1–6], these quantities were not still high enough because of the nonselective gas phase reactions induced by the catalyst surface [7]. Several studies on OCM were carried out in packed-bed reactors in co-feed operation mode in which methane and oxygen were fed to the reactor at the same time [8–15]. The main drawback of these studies (co-feed operation) is the low C_2 selectivity as the total oxidant of the process is gaseous molecular oxygen [16–17]. To solve this problem, researchers shifted to use membrane reactors, which provide the indirect mixing of methane and oxygen via transport of molecular oxygen in the form of ionic oxygen species [18–25]. The major advantage of membrane reactor is preventing the direct mixing of oxygen and methane.

The oxygen permeable perovskites have the general formula of ABO_3 in which A is composed of rare and alkaline earth metal ions and B is a transition metal ion [26]. Substitution of alkaline-earth ions on the A-site affects the oxygen nonstoichiometry of the perovskite [16], while B-site can optimize the catalytic properties of the perovskite-type oxides for oxidation reactions [26,27]. Dense membranes of the type of $La_xSr_{1-x}Co_yFe_{1-y}O_{3-\delta}$ are conductors of both oxygen ion and electron [28–35]. High oxygen permeation fluxes through the several $La_xSr_{1-x}Co_yFe_{1-y}O_{3-\delta}$ perovskite membranes are reported, previously [36–37]. The higher Co and Sr contents in the perovskite result in higher oxygen flux values [36], while the presence of La is necessary for the stability of this type of material [7].

Extensive studies on the OCM process in the membrane reactors were performed taking into account: the catalytic properties

Abbreviations: OCM, oxidative coupling of methane; EDTNAD, ethylene diamine *N*,*N*,*N*′,*N*′-tetra *N*-acetyl diamine; GC, gas chromatography.

* Corresponding author. Tel.: +98 21 44438526; fax: +98 21 55932428.
E-mail address: nazarikh@ripi.ir (K. Nazari).

1381-1169/$ – see front matter © 2008 Elsevier B.V. All rights reserved.
doi:10.1016/j.molcata.2008.01.043

of perovskite-type [18,20], tubular membrane [38–41], packed catalyst in the tubular membrane reactor [41], the effects of oxygen flux, temperature and feed concentration [42] and the comparison of the membrane reactor with co-feed reactor [7,20].

Various procedures and method such as coprecipitation [43], solid-state reaction [44–47], combustion [48], citric-EDTA complexation [49–52] and sol–gel process [53] were introduced for synthesis of perovskite powders. The quality of produced powder depends on the preparation method. Perovskite-type oxide $La_{0.6}Sr_{0.4}Co_{0.8}Fe_{0.2}O_{3-\delta}$ produced by EDTA method and its application as a dense membrane for OCM process is previously reported [54].

In the present work, a new facile complexation procedure in preparation of LSCF perovskite membrane is described. The advantages of the method are described and the catalytic behavior of dense membrane ($La_{0.6}Sr_{0.4}Co_{0.8}Fe_{0.2}O_{3-\delta}$) is studied in the oxygen permeation and OCM reaction. Furthermore, the OCM reaction is investigated in the fixed-bed reactor with the packed perovskite catalyst and the comparative results were obtained and discussed for the fixed-bed and membrane reactors.

2. Experimental

2.1. Materials

$Sr(NO_3)_2$ (with the purity of 99%), $Co(NO_3)_2{\cdot}6H_2O$ (97%), $Fe(NO_3)_3{\cdot}9H_2O$ (98%) and $La(NO_3){\cdot}6H_2O$ (99%) were purchased from Merck and used without further purification. Pure ethylene diamine *N*,*N*,*N*′,*N*′-tetra *N*-acetyl diamine (EDTNAD) obtained from Research Institute of Petroleum Industry and was used as a 70% solution in water [55]. All of the salts solutions were prepared in CO_2-free deionized water (Barnstead NANO pure D4742 deionizer, Electrical Resistance = 18.3 MΩ).

2.2. Instrumentations

A programmable tubular furnace (Heraeus model RO 4/50) was used for calcinations of perovskite powders at 1223 K. Another programmable chamber furnace (Lindberg model 59744) was also used for sintering of the perovskite catalyst at 1473 K.

An on-line gas chromatograph (GC, model Chrompack 9000), which was equipped with a 13× molecular sieve column, thermal conductivity and flame ionization detectors. An auto-sampling valve was used to online analysis of the products and permeated gas by GC. The flow rates of the inlet gases were also controlled by the digital mass flow controllers (Brooks 5850), which were calibrated by a 10 ml bubble flow meter.

The crystal structure of the membrane samples was characterized by X-ray diffraction (XRD) (Philips-PW model 1840, with CU Kα radiation) with a 2θ scan from 20° to 70°. The morphology of the membrane was examined by scanning electron microscopy (SEM) technique (Cambridge model S360). Experimental formula and stoichiometry of the metal ions for the prepared perovskite were determined and confirmed by atomic absorption spectroscopy (Perkin-Elmer AA 200) and Inductively Coupled Plasma (ICP, Plasma 400) techniques. A Hach laboratory turbidimeter model 2100N was used for measurement of turbidity of the solutions.

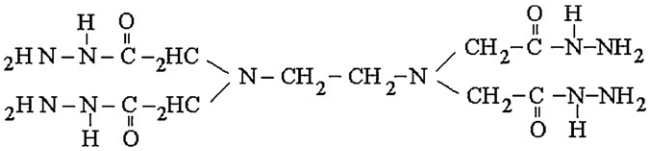

Ethylene Diamine N,N,N',N'-Tetra N-Acetyl Diamine (EDTNAD)

Scheme 1. Structure of EDTNAD ligand.

2.3. Preparation of LSCF membranes

EDTNAD with the structure shown in Scheme 1 is a ligand consisting of four hydrazide groups and has the capability of strong complex formation with alkaline earth and transition metal ions and even is able to easily dissolve the oxide forms of the metals at neutral pH [55].

The $La_{0.6}Sr_{0.4}Co_{0.8}Fe_{0.2}O_{3-\delta}$ (LSCF) powder was prepared by complexation method with EDTNAD solution. In this method stoichiometric amount of each salt including $Sr(NO_3)_2$, $Co(NO_3)_2{\cdot}6H_2O$, $Fe(NO_3)_3{\cdot}9H_2O$ and $La(NO_3){\cdot}6H_2O$ were first dissolved in a 18% (V/V) EDTNAD aqueous solution. The obtained solution was heated at 333 K for about 3 h while stirring. The obtained gel-like dark-red material by evaporating the solution at room temperature is then self-ignited at 473 K in a vacuum oven. Then, the obtained gray powder was calcined at 1223 K for 5 h. The obtained black oxide powder was pressed into disk pellets under 400 MPa (4000 bar) hydraulic pressure. Disks were sintered at 1473 K for 10 h by heating and then cooling rate at 2 K/min. Both sides of the sintered membrane were polished with 1000 mesh SiC paper to give a final thickness of approximately 0.7–1.0 mm. Scheme 2 shows the stepwise diagram for preparation the LSCF disk membrane. The perovskite phase structure of the samples was characterized by X-ray diffraction.

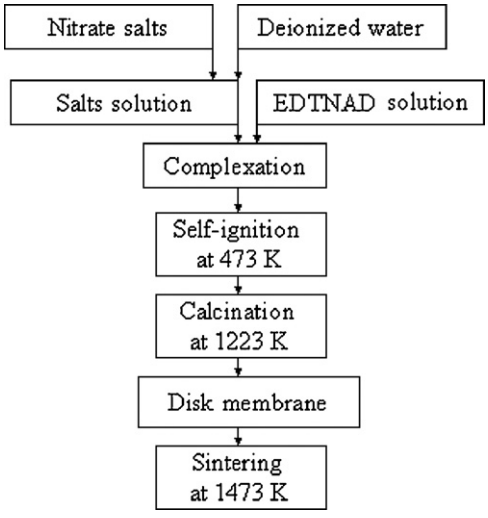

Scheme 2. The diagram of preparation steps for LSCF disk membrane perovskite.

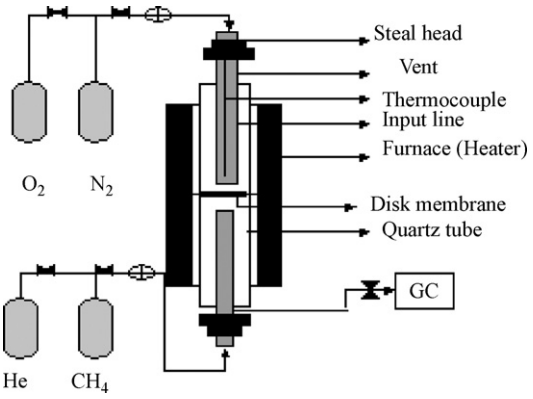

Scheme 3. The membrane reactor setup for oxygen permeation and OCM reaction studies.

2.4. Membrane and fixed bed reactor setup and procedures

Scheme 3 shows the overall appearance of the membrane reactor apparatus. One side of the membrane was exposed to a mixture of O_2–N_2 and/or air and the other side exposed to either diluted methane in the OCM reaction run, or helium in the permeation run. The prepared perovskite membrane with about 11 mm diameter was placed between two quartz tubes (12.0 mm outer diameter, 11.0 mm inner diameter), which were sealed by two Pyrex rings.

Two parts of the membrane reactor (upper and lower parts) were fixed by two steel heads outside the small tubular furnace of the setup shown in Scheme 3. The small tubular furnace (Heraeus HANAU) equipped with a controller was used to adjust and read the reaction temperature (with a K-type thermocouple). In order to seal the quartz membrane reactor around the disk, it was fixed between two Pyrex rings, heating at 1223 K. To check the successful sealing, helium and nitrogen streams were respectively introduced through lower and upper sides of the membrane. The complete sealing corresponds with no detection of nitrogen in the effluent of the helium stream by GC. Two steel heads (see Scheme 3) supplied and conducted methane–helium as well as oxygen and nitrogen mixture gases to both sides of the perovskite disk, separately. A thermocouple was inserted into the quartz tube (4 cm above the disk) for measuring the temperature. The permeate stream was cooled to room temperature for monitoring the composition of the product stream and then analyzed by GC. The oxygen permeability measurements were done by exposing one side of the membrane to a mixture of O_2–N_2 and/or air (150 ml/min), while the other side was only exposed to helium (25 ml/min). In the case of OCM reaction, oxygen (25 ml/min) was introduced through one side, while diluted methane with helium (80 ml/min) flowing through other side of the membrane. In the case of co-feed reactor, OCM reaction was carried out in a tubular fixed bed micro-reactor using a quartz tube (6 mm inner diameter) in the said small tubular furnace and atmospheric pressure. The mixture of methane, oxygen and helium with flow rate of 80 ml/min was exposed as feed to the reactor. The feed stream passed through the sieved catalyst (0.5 gr, 30–35 mesh). The reaction temperature was controlled by a controller and measured using a K-type thermocouple placed under the catalytic bed. Product stream was withdrawn from the bottom of tubular reactor and analyzed by GC.

3. Results and discussion

3.1. Comparison of homogeneity of the solutions of EDTA and EDTNAD metal complexes

In order to indicate the higher potential of the new chelating agent, EDTNAD, two experiments were conducted for comparing the homogeneity and pH-stability of the metal complexes. 8.0676 gr of H_4-EDTA (ethylene diamine tetra acetic acid) was dissolved in ammonia solution (8.0 M). The pH of this solution was about 8. Then stoichiometric amounts of metallic nitrates $Sr(NO_3)_2$, $La(NO_3)\cdot 6H_2O$, $Co(NO_3)_2\cdot 6H_2O$ and $Fe(NO_3)_3\cdot 9H_2O$ were added, respectively so that the molar ratio of EDTA to total metal cation content was 1.5:1.0. After addition of the second salt, some coagulated materials formed in the solution. Indeed after addition of the metal salts, pH of the solution decreases considerably (becomes acidic). By heating and addition of excess amount of ammonia solution coagulates dissolved. The same problem was faced with the addition of 3rd and 4th salts in which small size particles were formed in the solution. Again using heat and extra amount of ammonia solution the problem was solved. These findings indicate that the metal ions/EDTA complexes do not show high stability with the changes in pH of the solution and the solution is not really homogeneous probably because of partial formation of metallic hydroxides at alkaline pHs. To check the homogeneity of the solution at high pH values, turbidity of the solutions at pH 8.0 and pH 12.0 were measured using a Hach laboratory turbidimeter. Turbidity of the solutions was obtained 95 and 57 NTU (Nephelometric Turbidity Units), respectively. At pH 3.0 the solution was containing large amounts of coagulates and precipitates.

In the second experiment, a solution of metal ions/EDTNAD with a molar ratio of EDTNAD to total metal cation content of 1.5:1.0 was prepared. Using the EDTNAD chelating agent none of the above problems were observed. The solution was clear and homogeneous at acidic and alkaline media. For example turbidity of the complex solutions of metal ions/EDTNAD at pH 3.0, pH 8.0 and pH 12.0 were obtained 4, 2 and 1 NTU, respectively. EDTNAD chelating agent can also use as a potent descaler, which can even dissolve iron oxides of Fe_2O_3 and Fe_3O_4 [55].

3.2. Characterization of the membrane material

XRD technique provides an effective and direct way to characterize the phase structure of the prepared perovskites. Pattern a in Fig. 1 shows the crystal phase of the prepared LSCF via the EDTNAD synthesis method (Scheme 2), which is similar to that previously reported by Elshof and coworkers [54]. Fig. 1 shows the XRD patterns of the perovskite at room temperature after calcinations at 1223 K (pattern a) and sintered at 1473 K (pattern b), respectively. Calcination at higher temperatures shows the presence of an essentially pure perovskite phase. Pattern c is the crystal structure of LSCF perovskite (sin-

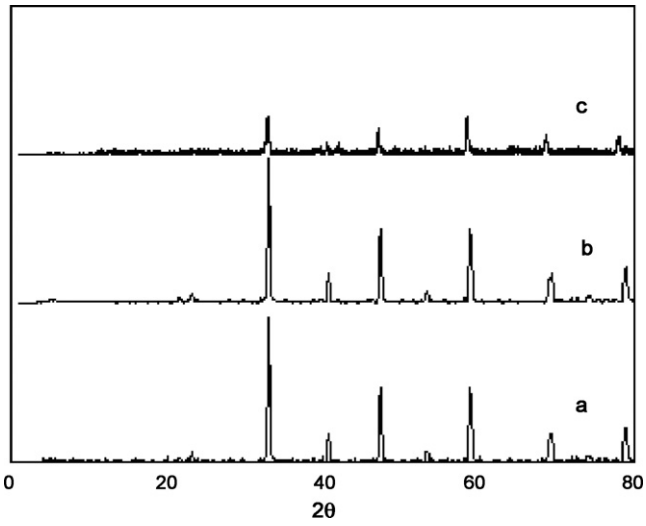

Fig. 1. XRD patterns of the LSCF perovskite: (a) calcined at 1223 K; (b) sintered at 1473 K; (c) sintered sample after treating by O_2 for 12 h.

tered at 1473 K) after the oxygen permeation experiments. The XRD pattern c indicated that exposing the membrane surface to oxygen for about 12 h (at 1073–1173 K) led to lowering the intensity and broadening of peaks, which is corresponding to a decrease in the crystallite size of the perovskite phase. Similar results is shown for oxygen permeability and stability of LSCF perovskite membranes, in which partial transformation of LSCF to the metal oxides associated with a decrease in the crystallite size of the perovskite is reported [56]. The crystallite sizes of the catalyst membranes were determined from the XRD data using Scherrer relation [57]. The crystallite size of the perovskite membrane was obtained 60 and 12 nm before and after oxygen permeation, respectively. As the pattern c shows, main peaks positions remained unchanged, which means LSCF perovskite phase is still thermally stable and did not change considerably after treating by oxygen (see Fig. 1). In accordance to the XRD patterns and crystal size determination data, clearly no transition from the crystal to the amorphous phase can be detected. Fig. 2a and b shows the SEM images of the LSCF perovskite after calcinations at 1223 K and sintering at 1473 K, respectively. When the sintering temperature is low (1223 K),

Table 1
Elemental analysis by atomic absorption and ICP for the prepared perovskite

Composition (%W/W)	$La_{1-x}Sr_xCo_yFe_{1-y}$
La	37.0
Sr	15.5
Co	18.3
Fe	4.9

the perovskite is partially porous because of complete burning of the ligand. Sintering at higher temperatures (1473 K) led to a dense membrane with distinct boundaries and grown grains. The elemental analysis of the prepared LSCF membrane is shown in Table 1. The density of the membrane was measured by means of Archimedes method. The relative density was 96.5% of theoretical.

The nonstoichiometry of $La_{0.6}Sr_{0.4}Co_{0.8}Fe_{0.2}O_{3-\delta}$ (LSCF) at room temperature (δ_{RT}) was determined using the oxidizing power method [58] which is described elsewhere [59]. First, the LSCF powder was heated to 1000 °C and slowly cooled in air (150 °C/day) to the room temperature. Then the powder was dissolved in a 2 M HCl solution. Chloride anion reduces Fe and Co to their 3^+ and 2^+ oxidation states, respectively. The released Cl_2 in the reduction step was conducted to a potassium iodide (KI) solution in which chlorine oxidizes I^- to I_2. The amount of iodine was determined by redox titration using standard sodium thiosulfate (as the titrant solution) from which the average valency of the transition metal cations and the oxygen nonstoichiometry can be calculated.

Generally, it is believed that the nonstoichiometry at a given oxygen pressure and temperature decreases with iron content of the perovskite [60]. At low δ values, the oxygen chemical potential decreases with δ. This observation is corresponding to the random distribution of oxygen vacancies. At high values of δ, partial decomposition of the perovskite phase occurs. Hence, we used a dense membrane perovskite with low Fe content for a better structural stability [61]. Iodometric titration result showed a value of $\delta \sim 0.017$ at ambient temperature for the used LSCF from which it is concluded the LSCF to be stoichiometric. Similar results were reported for a LSCF with even higher iron content ($La_{0.6}Sr_{0.4}Co_{0.2}Fe_{0.8}O_{3-\delta}$) [59].

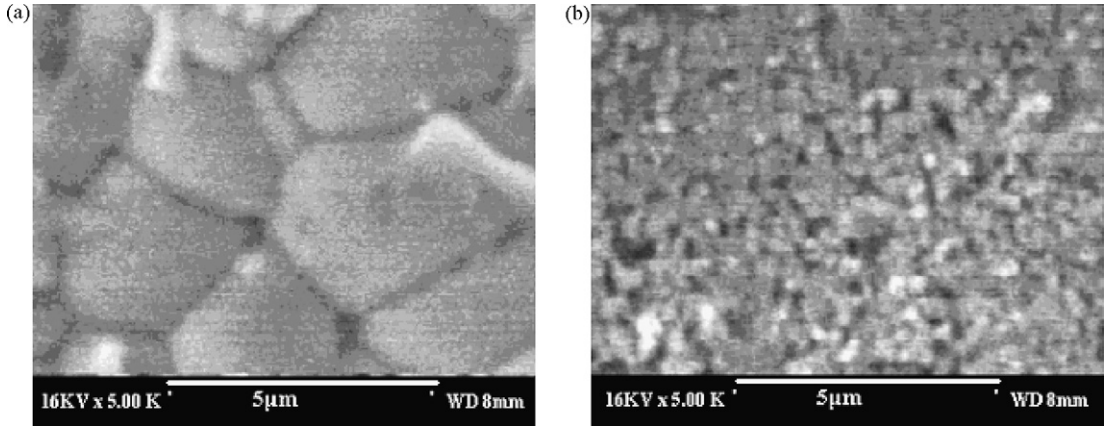

Fig. 2. SEM images indicating surface morphology of the LSCF perovskite sintered at: (a) 1473 K and (b) 1223 K.

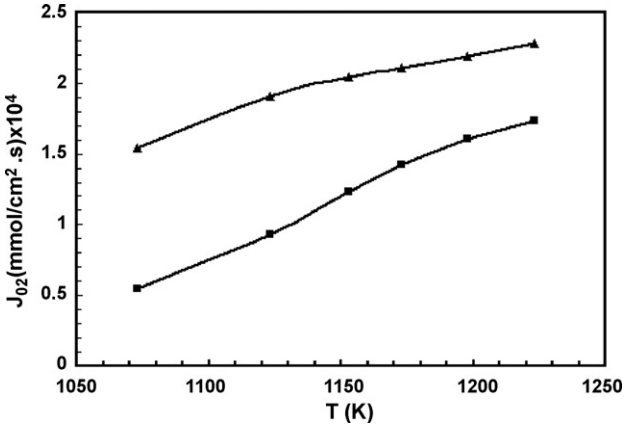

Fig. 3. Oxygen flux through the LSCF disk as a function of temperature for two thickness values of the membrane ($P_{O_2} = 0.21$ bar). (▲) $L = 0.75$ mm and (■) $L = 0.85$ mm.

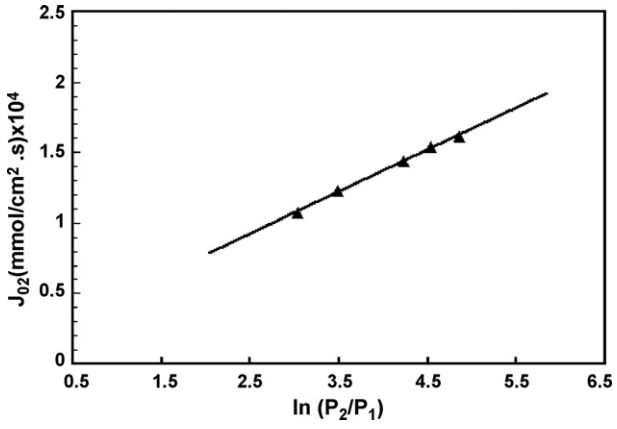

Fig. 4. Oxygen permeation flux through the LSCFO membrane disk as a function of $\ln(P_2/P_1)$, $T = 1153$ K, $L = 0.85$ mm, $P_2 = 0.1$–1 bar.

3.3. Oxygen permeability of the LSCF membrane

Temperature dependence of oxygen permeation flux through the $La_{0.6}Sr_{0.4}Co_{0.8}Fe_{0.2}O_{3-\delta}$ membrane was examined as shown in Fig. 3. According to the figure, the oxygen permeation flux increases with increasing of temperature. The oxygen ion diffusion rate in the bulk lattice is driven by the pressure difference and the tendency of increase in oxygen flux with the elevating temperature is due to the increase of mobility and concentration of ionic carriers at high temperature. In order to change oxygen partial pressure over range of 0.1–1.0 bar, oxygen and nitrogen gases were mixed with different proportions in the feed side. By applying an oxygen partial pressure gradient across the membrane, oxygen is driven from the high partial pressure side to the low partial pressure side. Two processes can describe the oxygen transport: the surface exchange reactions on the membrane surfaces and the ionic diffusion through the bulk material.

The characteristic thickness parameter, L_c, as the ratio of the oxygen diffusivity to the surface exchange coefficient can be used to specify the type of permeation through perovskite membranes [51]. When the membrane thickness is greater than L_c, the oxygen flux would be mainly controlled by the bulk diffusion rate, whereas for thickness $<L_c$, the oxygen flux would be limited by the mixed effects of surface exchange kinetics and the bulk diffusion rate. If the bulk diffusion effect controls the oxygen permeation, then the oxygen permeation flux (J_{O_2}) of the membrane can be described by the following relation [61]:

$$J_{O_2} = \frac{RT}{16F^2L}\left(\frac{\sigma_i \times \sigma_e}{\sigma_i + \sigma_e}\right)\ln\left(\frac{P_2}{P_1}\right) \quad (1)$$

where L (cm) is the membrane thickness, P_1 (bar) and P_2 (bar) are the low and high oxygen partial pressures on the two sides of membrane, respectively. σ_i and σ_e (S cm^{-1}) indicate the oxygen ion conductivity and electron conductivity of the perovskite membrane, R and T (K) are the gas constant and temperature, respectively.

According to Eq. (1), for bulk diffusion of oxygen permeation a linear plot of oxygen permeation flux (J_{O_2}) versus $\ln(P_2/P_1)$ would be expected as shown in Fig. 4. Furthermore, oxygen permeation flux decreases with increasing membrane thickness from 0.75 to 0.85 mm as shown in Fig. 3. Eq. (1) and Fig. 3 indicate that oxygen permeation flux is inversely depended on the membrane thickness [54].

Fig. 5 shows variation of oxygen flux with partial pressure of permeated oxygen at helium flow rates of 5(inset) and 25 ml/min. The existence of N_2 gas provides a good tool to check the successful sealing and/or cracking of the membrane. Oxygen/nitrogen mixtures with a constant flow rate of about 150 ml/min were used and no detectable nitrogen was observed in the permeate side of the membrane during these measurements. Above 1240 K the Pyrex sealing rings melted and spread on the disk surface leading to disrupting the sealing of membrane reactor.

Increasing the helium sweep flow rate in the permeate side result in reducing the oxygen partial pressure and increasing the oxygen permeation flux, which is normally expected for dilution of a gas mixture at constant pressure (here, atmospheric pressure).

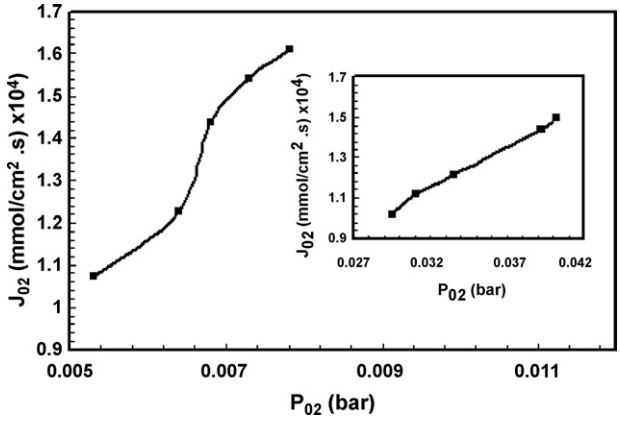

Fig. 5. Oxygen flux through the LSCF disk as a function of P_{O_2} at helium flow rate of $F_{He} = 25$ ml/min and $F_{(O_2+N_2)} = 150$ ml/min, membrane thickness (L) = 0.85 mm and $T = 1153$ K. Inset: Oxygen flux through the LSCF disk as a function of P_{O_2} at helium flow rate of $F_{He} = 5$ ml/min and $F_{(O_2+N_2)} = 150$ ml/min, membrane thickness (L) = 0.85 mm and $T = 1153$ K.

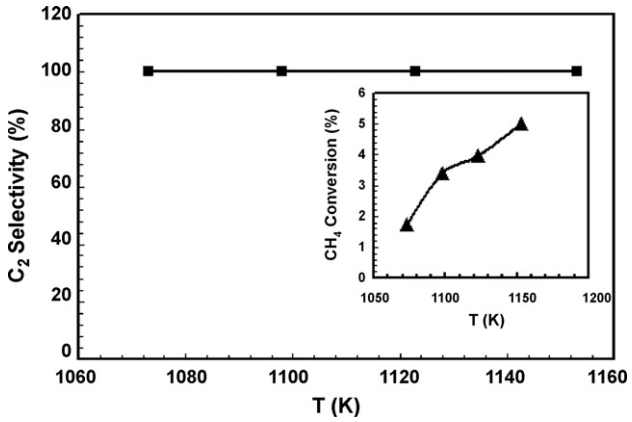

Fig. 6. C_2 selectivity plot as a function of temperature for the membrane LSCF catalyst, at the total flow rate of 80 ml/min. Inset: CH_4 conversion plot as a function of temperature for the membrane LSCF catalyst, at the total flow rate of 80 ml/min.

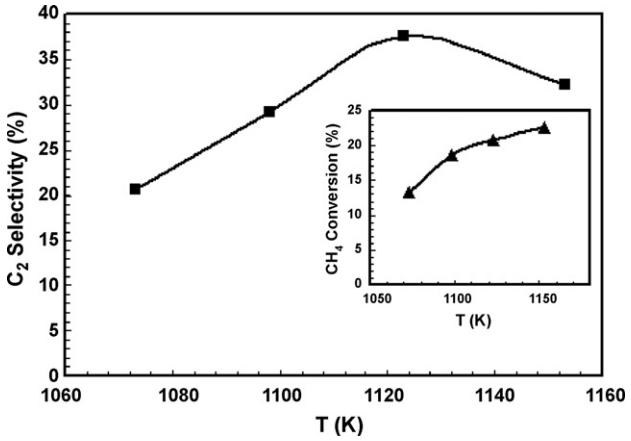

Fig. 7. C_2 selectivity plot as a function of temperature for the fixed-bed LSCF catalyst, at the total flow rate of 80 ml/min. Inset: CH_4 conversion plot as a function of temperature for the fixed-bed LSCF catalyst, at the total flow rate of 80 ml/min.

3.4. Oxidative coupling of methane (OCM) using the LSCF membrane and fixed bed reactor

OCM reactions were carried out in the LSCF dense membrane reactor shown in Scheme 3. A mixture of He and CH_4 was fed on one side and oxygen on the other side. Experimental results obtained from the membrane reactor were compared with those of fixed bed reactor at temperature range of 1073–1223 K. The best results including C_2 selectivity, conversion and yield were obtained at temperature range of 1073–1153 K.

Below 1073 K the extent of oxygen permeation is low and above 1240 K the sealing of membrane reactor was lost, hence the values of C_2 selectivity is only reported for the above optimum temperature range. Figs. 6 and 7 show the plot of the C_2 selectivity and methane conversion versus temperature for both of the membrane and fixed-bed reactors. Fig. 6:inset represents a maximum methane conversion of 5.01% for the membrane reactor while the maximum conversion for the fixed-bed reactor was obtained 22% as shown in Fig. 7: inset. It must be mentioned that in the OCM reaction the low conversion is not a limiting factor, instead, the higher C_2 selectivity is of paramount importance because in contrast to the fixed-bed catalyst, the membrane catalyst showed no methane combustion (CO_x formation reactions). The comparative data of Figs. 6 and 7 were obtained at the similar conditions of: (a) the amount of catalyst, (b) the temperature range and (c) the feed flow rates. Since the catalytic nature of the two processes are different [54], hence the conversion values are not in the same range meaning that it is not possible to compare the results of the two processes at a similar conversion value. As the figures show, C_2 selectivity, as the most important parameter for OCM reaction, for the LSCF dense membrane was found to be about 100% over the used temperature range of 1073–1153 K (Fig. 6), while the maximum value of C_2 selectivity for the same perovskite powder in the fixed bed reactor (co-feed operation) was obtained about 37% (Fig. 7). In the fixed-bed reactor, upon direct mixing of methane and oxygen different products including CO_x could be obtained. This indicates that the nature of the catalyst is different in the membrane mode and co-feed mode of operation, due to the presence of various active oxygen species at the surface [54].

It must be mentioned that, at high temperatures (typically $T > 1153$ K) and in the absence of molecular oxygen, thermal decomposition of CH_4 to carbon results in formation of $SrCO_3$ even in the absence of CO_2 [54]. Slow formation (within about 200 h) of $SrCO_3$ up to 80 nm depth of membrane is confirmed by the Auger and SEM analysis, while the membrane still has been stable [54]. Furthermore, in the presence of molecular oxygen and at $T > 1170$, C_2 selectivity for LSCF membrane strongly decreases [54]. Over the temperature optimum range of our experiments (1073–1153 K) no GC-detectable CO, CO_2 and/or molecular oxygen were measured while in the case of fixed-bed reactor, considerable amounts of CO_2 were detected as reflected in Fig. 7. The above results illustrate the preferable use of membrane reactor (in comparison to the fixed-bed) to achieve high

Table 2
Effect of temperature on the OCM performance in LSCF membrane and fixed-bed reactors

T (°C)	Membrane reactor			Fixed-bed reactor		
	C_2 selectivity (%)	$[C_2H_6]/[C_2H_4]$	$[C_2H_4]/[C_2]$	C_2 selectivity (%)	$[C_2H_6]/[C_2H_4]$	$[C_2H_6]/[C_2]$
1073	100	2.00	0.66	20.7	0.77	0.44
1098	100	2.00	0.66	29.2	0.51	0.35
1123	100	3.55	0.78	37.5	0.30	0.21
1153	100	2.28	0.69	32.3	0.16	0.13

selectivity in the OCM reaction. As it could be inferred from Fig. 6, since in the methane side of the membrane reactor the anionic oxygen is the limiting reactant, thus it can easily activate the methane for the OCM reaction. Practically, by controlling the effective parameters, it is possible to minimize the concentration of permeated molecular oxygen and prevent the direct oxidation of methane to CO_x. Hence, the permeated ionic oxygen on the catalyst surface can produce the C_2 products. The comparative results including compositions of C_2H_6 and C_2H_4 and the relative concentrations of C_2H_6/C_2H_4 for both of the membrane and fixed-bed reactors over the temperature range of 1073–1153 K are shown in Table 2. As the table shows in the fixed-bed reactor, the amount of produced ethylene (in comparison to ethane) increases slowly with increasing temperature. However, in the case of membrane reactor, the amount C_2H_6 is more than C_2H_4 over the whole range of temperature and the relative concentration of C_2H_6/C_2H_4 shows a maximum at 1123 K.

Fig. 8 depicts the performance of LSCF dense membrane reactor toward OCM reaction at the suitable temperature range of 1073–1153 K. The C_2 yield increases up to about 5.01% at 1153 K. To our knowledge the maximum values previously reported for C_2 selectivity and CH_4 conversion for this disk membrane perovskite ($La_{0.6}$ $Sr_{0.4}Co_{0.8}Fe_{0.2}O_{3-\delta}$) over temperature range of 1073–1173 K were 70% and 3%, respectively [54]. Our experiences proved that a very good sealing around two sides of the membrane and the new synthesis procedure for the perovskite were the main important parameters to achieve very high C_2 selectivity in the OCM reaction.

Fig. 9 shows the oxygen permeation fluxes through LSCF membrane under OCM conditions and permeation experiment. Oxygen permeation in OCM was obtained by calculating the amount of oxygen consumed in the oxidation reactions, since no GC-detectable oxygen was found in the downstream [43]. Based on the results of Fig. 9, consumption of permeated oxygen in the presence of methane in the downstream gas enhances the oxygen flux 6–9 times as compared to the He case (in the absence of CH_4). Similar results were reported for the OCM reaction using the $La_{0.8}Sr_{0.2}Co_{0.6}Fe_{0.4}$ membrane perovskite [43].

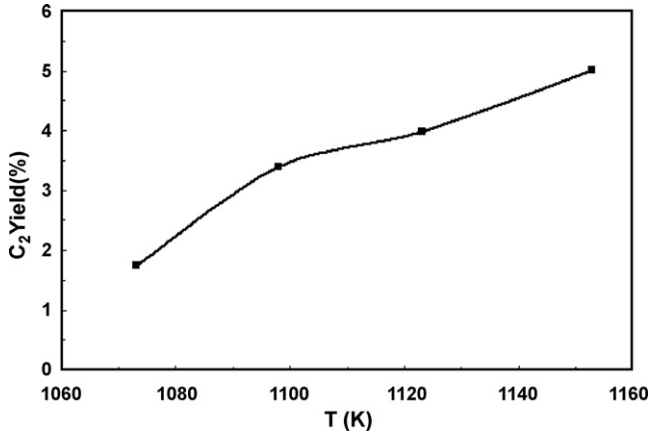

Fig. 8. C_2 yield in the OCM reaction as a function of temperature in the membrane reactor, total flow rate = 80 ml/min.

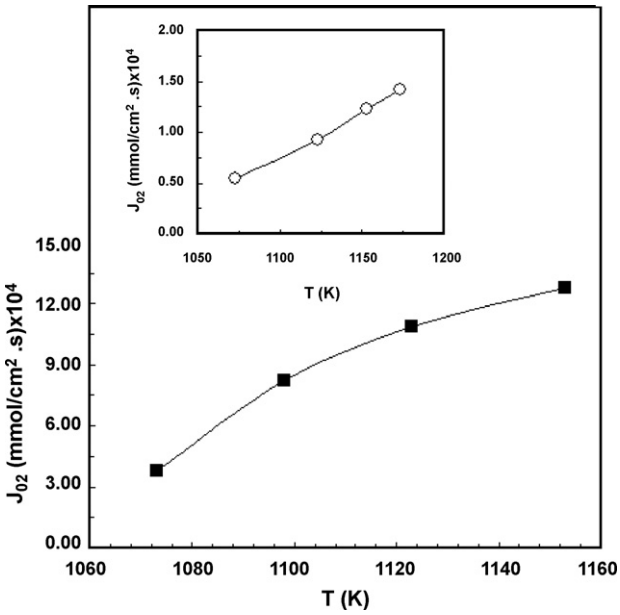

Fig. 9. Comparison of oxygen permeation fluxes through LSCF membrane. (◯) He and (■) OCM reaction (He/CH_4).

4. Conclusion

The new complexation agent ethylene diamine *N*,*N*,*N*′,*N*′-tetra *N*-acetyl diamine (EDTNAD) was successfully used for facile single-step preparation of homogeneous and stable complexes of the four metal ions including La^{3+}, Sr^{2+}, Co^{2+}, Fe^{3+}. The advantages of the method are:

1. Single step complex formation.
2. Homogeneity of the materials in both the aqueous solution and solid phase (see Section 3.1).
3. Stability of the formed complex at highly alkaline solutions and no need to control the pH of the solution with ammonia and/or citric acid in the synthesis method (see Section 3.1).
4. Simultaneous and strong complexation of the all metallic ions.

The subsequent prepared catalyst with a pure perovskite ($La_{0.6}Sr_{0.4}Co_{0.8}Fe_{0.2}O_{3-\delta}$) structure showed good oxygen permeability based on the bulk diffusion mechanism. Results showed that oxygen flux increases with decreasing thickness of the membrane and using a suitable flow of He in the permeate side, can facilitate the oxygen permeation through the membrane via sweeping and removing the permeated oxygen and regeneration of free surface to achieve a one-way oxygen permeation process. Using the LSCF disk for OCM reaction in the atmospheric membrane reactor conducted the process towards 100% C_2 selectivity and high yield (5.01%) at 1153 K.

Surface modification of the membrane by suitable promoters and thin porous layers of methane coupling catalysts such as Li/MgO may expect substantial improvements of the methane conversion. Also nanosized catalyst preparation, sandwiched perovskite between thermally stable porous supports and application of tubular membranes can be used to increase the total

supply of oxygen to the methane stream via enlargement of the surface area of the membrane. In addition to the mentioned objectives, kinetics and reaction mechanism of the catalyzed OCM reaction by the LSCF perovskite are in-progress and future research plans in this laboratory.

Acknowledgment

The financial support of the Research Institute of Petroleum Industry is gratefully acknowledged.

References

[1] G.E. Keller, M.M. Bhasin, J. Catal. 73 (1982) 9–19.
[2] M. Baerns, K. van der Wiele, J.R.H. Ross, Catal. Today 4 (1989) 471–494.
[3] A.M. Maitra, Appl. Catal. A 104 (1993) 11–59.
[4] N.D. Parkyns, C.I. Warburton, J.D. Wilson, Catal. Today 18 (1993) 385–442.
[5] J.S. Lee, S.T. Oyama, Catal. Rev. Sci. Eng. 30 (1988) 249–280.
[6] Y. Amenomiya, V.I. Birss, M. Goledzinowski, J. Galuszka, A.R. Sanger, Catal. Rev. Sci. Eng. 32 (1990) 163.
[7] Y. LU, A.G. Dioxon, W.R. Moser, Y.H. Ma, J. Membr. Sci. 170 (2000) 27.
[8] A.L. Tonkovich, R.W. Carr, R. Aris, Science 262 (1993) 221–223.
[9] S.C. Reyes, E. Iglesia, C.P. Kelkar, Chem. Eng. Sci. 48 (1993) 2643–2661.
[10] S.C. Reyes, C.P. Kelkar, E. Iglesia, Catal. Lett. 19 (1993) 167–180.
[11] J. Santamaria, J. Coronas, M. Menendez, Chem. Eng. Sci. 48 (1994) 4749–4757.
[12] M. Traykova, N. Davidova, J.Sh. Tsaih, A.H. Weiss, Appl. Catal. A 169 (1998) 237–247.
[13] J.H.B.J. Hoebink, P.M. Couwenberg, G.B. Marin, Chem. Eng. Sci. 49 (1994) 5453–5463.
[14] D. Schweer, L. Meeczko, M. Baerns, Catal. Today 21 (1994) 357–369.
[15] J. Da, X. Ding, Sh. Shen, Appl. Catal. A 116 (1994) 81–94.
[16] J. Mizusaki, Y. Mima, S. Yamauchi, K. Fueki, H. Tagawa, J. Solid State Chem. 80 (1989) 102–111.
[17] T. Akin, Y.S. Lin, AIChE J. 48 (2002) 2298–2306.
[18] S.J. Xu, W.J. Thomson, AIChE J. 43 (1997) 2731–2739.
[19] T. Nozaki, K. Fujimoto, AIChE J. 40 (1994) 870–877.
[20] J.E. ten Elshof, B.A. van Hassel, H.J.M. Bouwmeester, Catal. Today 25 (1995) 397–402.
[21] E.A. Hazbun, U.S. Patent 4,827,071 (1989).
[22] W. Wang, Y.S. Lin, J. Membr. Sci. 103 (1995) 219–234.
[23] Y.S. Lin, Y. Zeng, J. Catal. 164 (1996) 220–231.
[24] Y. Zeng, Y.S. Lin, J. Catal. 193 (2000) 58–64.
[25] J.H. White, E.A. Needhamm, R.L. Cook, A.F. Sammells, Solid State Ionics 53–56 (1992) 149–161.
[26] A.J. Burggraaf, L. Cot, Fundamentals of Inorganic Membrane Science and Technology, Elsevier, 1996.
[27] Z.P. Shao, G.X. Xiong, Y. Cong, W.S. Yang, J. Membr. Sci. 164 (2000) 167–176.
[28] A. Mai, F. Tietz, D. Stfver, Solid State Ionics 173 (2004) 35–40.
[29] D. Beckel, U.P.M.T. Gyger, G. Florey, A. Infortuna, L.J. Gauckler, Solid State Ionics 178 (2007) 407–415.
[30] Y. Teraoka, Y. Honbe, J. Ishii, H. Furukawa, I. Moriguchi, Solid State Ionics 152/153 (2002) 681–687.
[31] S.P. Scott, D. Mantzavinos, A. Hartley, M. Sahibzada, I.S. Metcalfe, Solid State Ionics 152/153 (2002) 777–781.
[32] Y.F. Liu, X.Q. Liu, G.Y. Meng, Mater. Lett. 48 (2001) 176–183.
[33] Sh. Li, W. Jin, N. Xu, J. Shi, J. Membr. Sci. 186 (2001) 195–204.
[34] W. Jin, Sh. Li, P. Huang, N. Xu, J. Shi, J. Membr. Sci. 185 (2001) 237–243.
[35] R.H.E.V. Doorn, A.J. Burggraaf, Solid State Ionics 128 (2000) 65–78.
[36] Y. Teraoka, H.M. Zhang, S. Furukawa, N. Yamazoe, Chem. Lett. (1985) 1743–1746.
[37] Y. Teraoka, T. Nobunaga, N. Yamazoe, Chem. Lett. (1988) 503–506.
[38] H. Wang, Y. Cong, W. Yang, Catal. Today 104 (2005) 160–167.
[39] Z. Shao, H. Dong, G. Xiong, Y. Cong, W. Yang, J. Membr. Sci. 183 (2001) 181–192.
[40] Y. Zeng, Y.S. Lin, Appl. Catal. A 159 (1997) 101–117.
[41] Y.K. Kao, L. Lei, Y.S. Lin, Ind. Eng. Chem. Res. 36 (1997) 3583–3593.
[42] X.M. Guo, K. Hidajat, C.B. Ching, H.F. Chen, Ind. Eng. Chem. Res. 36 (1997) 3576–3582.
[43] Y. Zeng, Y.S. Lin, S.L. Swartz, J. Membr. Sci. 150 (1998) 87–98.
[44] S. Li, W. Jin, N. Xu, J. Shi, Solid State Ionics 124 (1999) 161–170.
[45] B.J. Mitchell, R.C. Rogan, J.W. Richardson Jr., B. Ma, U. Balachandran, Solid State Ionics 146 (2002) 313–321.
[46] S. Lee, K.S. Lee, S.K. Woo, J.W. Kim, T. Ishihara, D.K. Kim, Solid State Ionics 158 (2003) 287–296.
[47] L. Yang, L. Tan, X. Gu, W. Jin, L. Zhang, N. Xu, Ind. Eng. Chem. Res. 42 (2003) 2299–2305.
[48] F.C. Buciuman, F. Patcas, J.C. Menezo, J. Barbier, T. Hahn, H.G. Lintz, Appl. Catal. A 35 (2002) 175–189.
[49] H. Lu, J. Tong, Y. Cong, W. Yang, Catal. Today 104 (2005) 154–159.
[50] J. Tong, W. Yang, B. Zhu, R. Cai, J. Membr. Sci. 203 (2002) 175–183.
[51] Z. Shao, G. Xiong, H. Dong, W. Yang, L. Lin, Sep. Purif. Technol. 25 (2001) 97–116.
[52] Z. Shao, G. Xiong, J. Tong, H. Dong, W. Yang, Sep. Purif. Technol. 25 (2001) 419–429.
[53] J. Liu, A.C. Co, S. Paulson, V.I. Birss, Solid State Ionics 177 (2006) 377–387.
[54] J.E. ten Elshof, H.J.M. Bouwmeester, H. Verweeij, Appl. Catal. A 130 (1995) 195–212.
[55] M. Kameli, K. Nazari, M. Zare, European Patent Office, Appl. No: 06000819.0 (2006).
[56] S. Li, W. Jin, P. Huang, N. Xu, J. Shi, Y.S. Lin, M.Z.C. Hu, E.A. Payzant, Ind. Eng. Chem. Res. 38 (1999) 2963–2972.
[57] B.D. Cullity, Elements of X-ray Diffraction, 2nd ed., Addison-Wesley Publishing Company, Inc., London, 1978.
[58] R.J. Nadalin, W. Brozda, Anal. Chim. Acta 28 (1963) 282–284.
[59] J.W. Stevenson, T.R. Armstrong, R.D. Carneim, L.R. Pederson, W.J. Weber, J. Electrochem. Soc. 143 (1996) 2722–2729.
[60] M.H.R. Lankhorst, J.E. ten Elshof, J. Solid State Chem. 130 (1997) 302–310.
[61] C. Wanger, J. Phys. Chem. B 21 (1933) 25.